INORGANIC CHEMISTRY
FRONTIERS

RESEARCH ARTICLE

View Article Online
View Journal | View Issue

Cite this: *Inorg. Chem. Front.*, 2022, **9**, 3071

Heptadentate chelates for ^{89}Zr-radiolabelling of monoclonal antibodies†

Amaury Guillou, [a] Ali Ouadi [b] and Jason P. Holland *[a]

Herein, we report the synthesis of three new bifunctional heptadentate metal ion binding chelates derived from desferrioxamine B (DFO) linked to a tripeptide unit that comprises of a glutamic acid and two glycine residues. The three DFO derivatives were also functionalised with a photoactivatable aryl azide unit for light-triggered labelling of proteins. The chelates were obtained in 3 synthetic steps in good overall yields by using solid phase peptide synthesis (SPPS). Density Functional Theory (DFT) calculations were used to estimate thermodynamic formation constants (log β) of the corresponding Zr^{4+} complexes. Quantitative zirconium-89 radiolabelling (>95%) was obtained in <5 min at room temperature, and the stability of the radioconjugates toward different competitors (human serum, EDTA and Fe^{3+}) was assessed *in vitro*. One-pot ^{89}Zr-photoradiosynthesis produced [^{89}Zr]Zr-**2**-onartuzumab directly from the formulated, clinical-grade sample MetMAb™, without pre-purifying the monoclonal antibody (mAb) component, with an isolated decay-corrected radiochemical yield of 36.4 ± 2.4%. PET imaging and biodistribution studies were performed in female athymic nude mice bearing subcutaneous xenografts derived from the MKN-45 human gastric cancer cell line to assess the pharmacokinetic profile and tumour binding of [^{89}Zr]Zr-**2**-onartuzumab. Specific tumour uptake of [^{89}Zr]Zr-**2**-onartuzumab was confirmed by using competitive inhibition (blocking) studies and bone uptake was significantly reduced compared to the parent DFO analogue.

Received 25th February 2022,
Accepted 10th May 2022

DOI: 10.1039/d2qi00442a

rsc.li/frontiers-inorganic

Introduction

Zirconium-89 (half-life: $t_{1/2}$ = 78.41 h, positron intensity: $I(\beta^+)$ = 22.3%) is a positron-emitting radionuclide that has risen to prominence for radiolabelling monoclonal antibodies (mAbs) for use in immuno-positron-emission tomography imaging (immuno-PET).[1,2] At present, more than 100 clinical trials are underway that utilise or test the performance of ^{89}Zr-mAbs as diagnostic imaging agents (**https://www.clinicaltrials.gov**). For applications in immuno-PET, the metalloradionuclide $^{89}Zr^{4+}$ ion needs to be sequestered by a ligand to form a coordination complex that is thermodynamically, kinetically, and metabolically stable in biological systems.

Due to its classification as a hard Lewis acid according to the Pearson theory, the Zr^{4+} ion has strong affinity for hard bases, and particular those bearing oxygen-based donors.[3] In its cationic form, Zr^{4+} can be engaged in coordination complexes by ligands bearing between 6 to 8 donor atoms. Desferrioxamine B (DFO), a natural bacterial siderophore, is an outstanding hexadentate linear chelator for zirconium-89, and clinical trials with ^{89}ZrDFO-radiolabelled antibodies have proven that the complex is suitable for use in human immuno-PET.[4,5] Nevertheless, preclinical studies have demonstrated that ^{89}ZrDFO-mAbs can suffer from dissociation and metal ion release *in vivo* resulting in partial bone uptake in mice.[6–8] The mechanism of demetallation *in vivo* remains unknown but is potentially due to the fact that the coordination sphere of the metallic cation is not fully completed with the DFO ligand (coordination number: CN = 6). Over a decade ago, we used Density Functional Theory (DFT) calculations to illustrate that the ZrDFO complex can potentially accommodate two additional water molecules as ligands.[9] These water molecules can bind in either pseudo-axial or pseudo-equatorial sites, whereby axial binding was predicted to be more stable, leading to an octadentate cationic complex $[Zr(DFO)(H_2O)_2]^+$.[9] In 2013, Guérard *et al.*[10] studied the coordination properties of Zr^{4+} ions with bidentate *N*-methyl acetohydroxamic acid ligand (Me-AHA) in solution and solid state by the mean of potentiometric titration and single crystal X-ray diffraction. The authors reported that the neutral, octadentate ML_4 species, [Zr(Me-AHA)$_4$], has a high thermodynamic stability constant (log β = 45.98) and the single crystal X-ray structure highlighted the octadentate environment around the metallic cation with a

[a]*University of Zurich, Department of Chemistry, Winterthurerstrasse 190, CH-8057 Zurich, Switzerland. E-mail: jason.holland@chem.uzh.ch; Tel: +41.44.63.53.990*
https://www.hollandlab.org
[b]*Université de Strasbourg, CNRS, IPHC UMR 7178, F-67000 Strasbourg, France*
† Electronic supplementary information (ESI) available. See DOI: **https://doi.org/10.1039/d2qi00442a**

cis,*trans*,*trans* configuration of the four Me-AHA ligands. We note that some debate exists regarding the experimental model used for the potentiometric determination of these constants.[11,12] Similar debate around potentiometric models derived for more elaborate zirconium complexes, and especially ZrDFO, has also arisen in the past few years, highlighting the need for more work in the field.[13–15] We simply note here that the potentiometric modelling work on ZrDFO species by Toporivski *et al.* required only the use of classic and stoichiometrically precise ML species (1 : 1 ratio of Zr to DFO complexation), whereas the more elaborate models from Bianchi *et al.* required the inclusion of higher order M_xL_y species to fit the experimental data. To the best of our knowledge, no experimental evidence has been reported to substantiate the existence (or otherwise) of these more elaborate metal ion clusters. Recently, Racow *et al.* measured the hydration state of the ZrDFO complex by using variable-temperature mass spectrometry (VT-MS) in the gas phase.[16] They demonstrated that under their analytical conditions, the monohydrated $[ZrDFO(H_2O)]^+$ species can be observed. These experimental data are consistent with the original DFT prediction[9] that suggested at least one water molecule is tightly bound to the cation. No empirical evidence of a second water molecule in the inner sphere was found but this observation was also consistent with the DFT prediction that the pseudo-equatorial water ligand is labile. More recent calculations from our group,[17] and experimental data from others[18] have also contributed to the collective understanding of ZrDFO coordination chemistry. The ZrDFO complex exhibits extensive geometric and stereoisomerism – the hexadentate species alone can potentially form 8 geometric isomers, each of which is chiral.[17] Addition of one or two coordinated water ligands expands the number of coordination species, and as Summer *et al.*[18] reported, one must also consider the formation of the hydroxide complexes from potential deprotonation of the aquo ligands.

Driven by the goal of increasing the stability of the $^{89}Zr^{4+}$ coordination complex toward demetallation *in vivo*, several groups around the world have explored the synthesis and coordination chemistry of novel multidentate chelates with coordination numbers from 6 to 8. Recent progress on aqueous-phase Zr-coordination chemistry has been reviewed extensively.[19–22] For new ligands to be useful in ^{89}Zr-radiochemistry, the compounds must have a reactive handle that allows bioconjugation to a protein (or other biologically active vector) of interest. Classical antibody functionalisation typically involves amide bond formation using *N*-hydroxysuccinimide (NHS) groups or thiourea synthesis from chemicals bearing benzyl isothiocyanate (NCS) groups.[23] These methods require a two-step approach where the mAb must be pre-purified from the formulation buffer prior to the bioconjugation step and subsequent radiolabelling. Although successful, these two-step methods are time consuming, cost intensive, and usually require harsh chemical conditions that potentially compromise the protein structure and binding properties. As an alternative method for functionalising mAbs with radiometal ion complexes, our group has developed a one-pot photochemical approach.[24–28] These new *PhotoTags* bear a photochemically active aryl azide (ArN_3) and can be used to modify mAbs with radiometal ion complexes for PET, and with fluorophores for optical imaging *in vitro* or *in vivo*.[29] Upon irradiation, the ArN_3 absorbs UV light at wavelengths where most proteins do not absorb (365–450 nm), hence avoiding photodegradation of the protein. Photon absorption forms a highly reactive electrophile (ketenimine intermediate) which further reacts with a nucleophile, such as the primary ε-NH_2 group of Lys residues present on the surface of antibodies, to form a new a covalent bond.[26,30] Remarkably, the phenomenon is compatible with various formulations buffers and can be fully automated.[31]

Here, we synthesised three new heptadentate DFO analogues (Fig. 1) bearing a discrete water-soluble tris-polyethylene glycol chain, a tripeptide (Gly-Gly-Glu) moiety, and a photoactivatable ArN_3 unit for light-induced protein ligation. The position of the carboxylate donor group was changed on the tripeptide motif to identify the optimum metal ion binding chelate based on stability studies *in vitro*. DFT calculations were used to predict the thermodynamic stability constants ($\log\beta$) of the complexes. The proligands were radiolabelled with $^{89}Zr^{4+}$ and the stabilities of the radiocomplexes were studied against various competitors. Based on the results, we selected the most stable complex and produced ^{89}Zr-radiolabelled onartuzumab (the monoclonal antibody component of MetMAb™ which binds to the human hepatocyte growth-

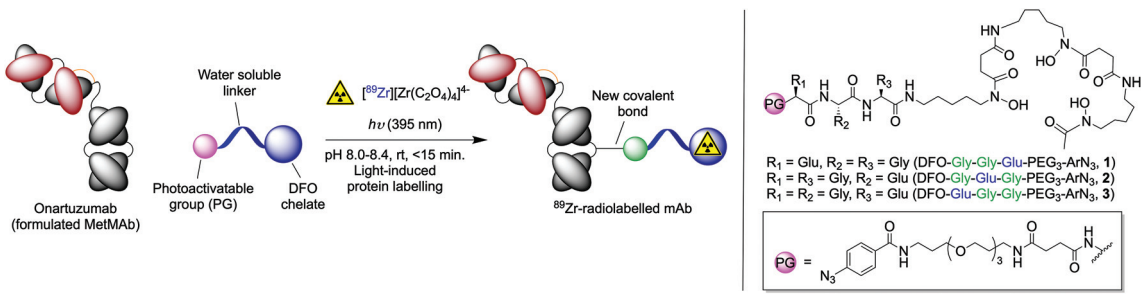

Fig. 1 Overview of the light-induced photoradiosynthesis to produce ^{89}Zr-labelled monoclonal antibodies (mAbs) and structure of the proligands (**1–3**).

factor receptor c-MET).[32] Finally, the pharmacokinetic profile and c-MET targeting of [^{89}Zr]Zr-**2**-onartuzumab was evaluated *in vivo* and *ex vivo* by using PET imaging and biodistribution studies in female athymic nude mice bearing subcutaneous MKN-45 human gastric cancer xenografts.

Results and discussion

Proligand synthesis

The synthesis of the three different photoactivatable heptadentate DFO analogues (**1–3**) is depicted in Scheme 1. The synthesis of DFO-PEG_3-ArN_3 (compound **4**) which is used as a hexadentate control is described elsewhere.[33] Full characterisation data including ^{1}H and $^{13}C\{^1H\}$ NMR spectra and high-resolution mass spectrometry (HRMS) are presented in the ESI (Fig. S1–S27†). Each of the three chelates (**1–3**) were obtained in 3 steps by using solid phase peptide synthesis methodologies. Briefly, sequential addition of either Fmoc-protected glycine or Boc-protected glutamic acid on 2-chlorotrityl resin generated the tripeptide units on resin. Then the photoactivatable ArN_3-PEG_3-NH-succ[33] group was coupled to the N-terminus. Cleavage from the resin was accomplished by using 1% TFA in CH_2Cl_2 to avoid deprotection of the *tert*-butyl ester. After C18 purification, the linear peptides (**6a**, 54%), (**6b**, 52%) and (**6c**, 28%) were obtained in high chemical purity (>95% by ^{1}H NMR spectroscopy). In a second step, the DFO metal binding chelate was introduced at the C-terminus of the peptides *via* a HATU-mediated amide coupling reaction to give compounds **5a**, **5b** and **5c** in yields ranging from 53% to 80%. Finally, the *tert*-butyl ester deprotections were carried out by using TFA/H_2O (1/1 v/v) and gave the final heptadentate metal binding chelates DFO-Gly-Gly-Glu-PEG_3-ArN_3 (**1**), DFO-Gly-Glu-Gly-PEG_3-ArN_3 (**2**), and DFO-Glu-Gly-Gly-PEG_3-ArN_3 (**3**), in 27%, 25% and 20% overall yield, respectively.

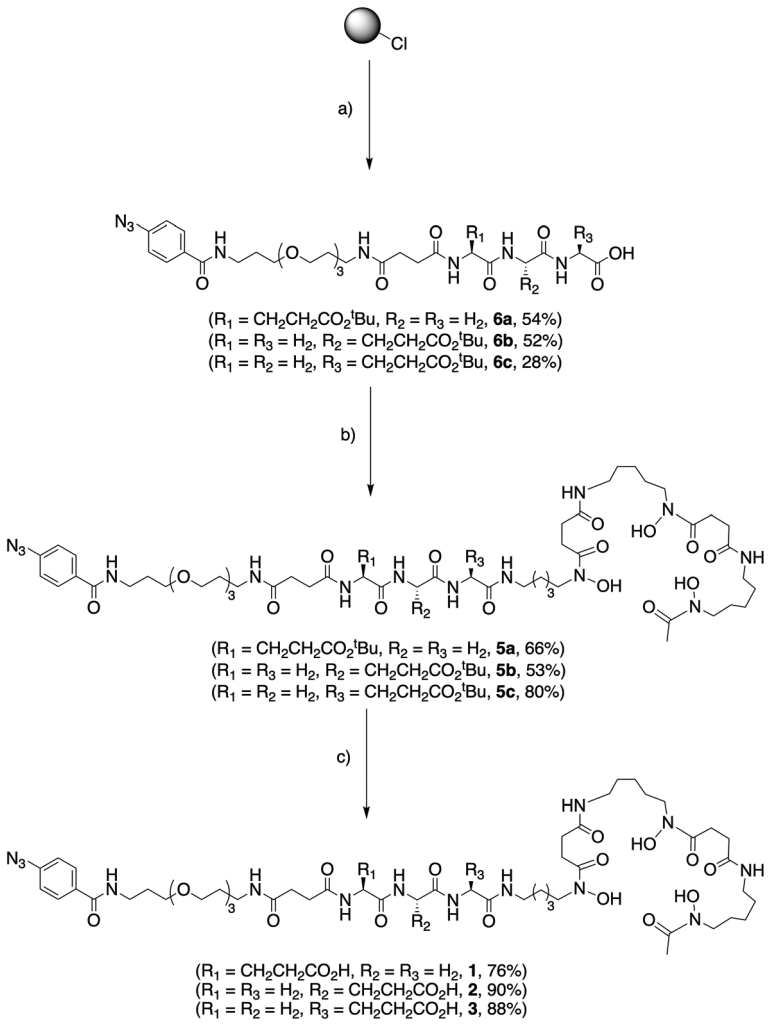

Scheme 1 General route for the synthesis of compounds **1–3**. (a) 2-Chlorotrytil resin, Fmoc-AA-OH (2 eq.), DIPEA (10 eq.), CH_2Cl_2, rt, 60 min. 20% piperidine/DMF, rt, 20 min. Fmoc-AA-OH (3 eq.), HBTU (2.9 eq.), DIPEA (6 eq.), DMF, rt, 90 min. Fmoc-AA-OH (3 eq.), HBTU (2.9 eq.), DIPEA (6 eq.), DMF, rt, 90 min. 20% piperidine/DMF, rt, 20 min. ArN_3-PEG_3-NHsucc (1.5 eq.), HBTU (2.9 eq.), DIPEA (6 eq.), DMF, rt, 90 min. 1% TFA/CH_2Cl_2, rt, 10 min. (b) HATU (1.5 eq.) DIPEA (4 eq.), DFO-mesylate (1.2 eq.), DMF, rt, 24 h. (c) TFA/H_2O, 120 min, rt.

Computational estimates of Zr-complex formation constants

To date, accurate experimental methods to measure the thermodynamic stability of Zr^{4+} complexes remain non-trivial. Due to its high charge-to-size ratio, Zr^{4+} ions form complexes with exceptionally high thermodynamic stability with formation constants $\log\beta > 30$.[34–37] Direct measurements of the formation constants of this magnitude are inaccessible to standard potentiometric titrations. The system is also complicated by the strong tendency of Zr^{4+} ions to hydrolyse or form polymeric oxides by olation under aqueous (and often mildly basic) conditions.[22] Therefore, batch processes and ligand competition methods are required, which pose the problem of choosing an adequate competitor ligand that produces a thermodynamically stable, yet kinetically labile metal ion complex with a well-defined formation constant for use as a reference. Another challenge to the experimental determination of thermodynamic formation constants is that the titrations often require large amounts (*ca.* >100 mg) of material. Synthesis of new chelates on this scale is not always possible.

To circumvent the aforementioned problems, we developed a straight-forward DFT-based computational method to predict the thermodynamic stability of Zr^{4+} complexes.[17] DFT calculations provide a rapid way of screening the relative stability of different complexes and can also aid the synthetic design of alternative new chelates. To simplify the calculations, model structures were used in which the desferrioxamine–tripeptide–PEG_3–ArN_3 structure was terminated with a methyl group instead of the PEG_3–ArN_3 moiety. This substitution is not anticipated to influence the overall thermodynamic stability of the complexes because the PEG_3–ArN_3 group is electronically decoupled from the metal ion centre and is spatially distal from the first coordination sphere of the Zr^{4+} ion. The model reaction is given by eqn (1) and the calculation of the estimated $\log\beta$ is given by eqn (2).[17]

$$[Zr(H_2O)_{19}]^{4+} + L^{b-} \rightleftharpoons [ZrL]^{(4-b)+} + 19(H_2O) \quad (1)$$

$$\log\beta_{estimated} = \frac{(\log\beta' - 45.48 \pm 2.47)}{1.985 \pm 0.095} \quad (2)$$

The aquated $[Zr(H_2O)_{19}]^{4+}$ ion includes 7 coordinated water molecules in the first coordination sphere and 12 water molecules in the secondary solvation shell. Full details of the structure and reference models have been reported in our previous computational work.[17] The optimised local structure of the model anionic ligand was calculated by first optimising the geometry of the equivalent Zr-complex, then removing the metal ion from the structure and reoptimising the des-metal anionic ligand. In all cases, only the most stable *N–cis–cis* isomer with respect to the coordination geometry of the DFO ligand around the Zr^{4+} ion was considered.[17] Based on this method the most stable 7-coordinate $[ZrDFO(H_2O)]^+$ complex had a calculated free energy change for metal ion complexation of $\Delta G = -726.5$ kJ mol^{-1}, resulting in an estimated formation constant $\log\beta = 41.20$.[17] This result is in excellent agreement with the experimental potentiometric studies of Toporivska *et al.* who reported a formation constant of $\log\beta = 40.40$.[15] The accuracy of the calculated result for the reference ZrDFO complex lends confidence in the ability of our DFT model to predict the thermodynamic stablity of other Zr^{4+} complexes.

Calculated thermodynamic data including the change in reaction free energy (ΔG/kJ mol^{-1}), enthalpy (ΔH/kJ mol^{-1}) and entropy (ΔS/J K^{-1} mol^{-1}) on complexation, and the estimated $\log\beta$ values for the formation of the neutral model Zr-complexes, Zr-**1**, Zr-**2**, Zr-**3**, and also ZrDFO-succinate,[17] are gathered in Table 1. The optimised structures of the model complexes are presented in Fig. 2.

For the ZrDFO-succinate complex, which is one of the simplest, readily accessible complexes that potentially exhibits 7-coordinate complexation to the central Zr^{4+} ion, the calculated free energy of complexation gave a value of $\Delta G = -774.9$ kJ mol^{-1} resulting in an estimated $\log\beta = 45.47$. Coordination of the carboxylate donor in the ZrDFO-succinate complex resulted in a $\log\beta$ value that is ~4 log unit higher than the most stable isomer of the 7-coordinate $[ZrDFO(H_2O)]^+$ complex ($\log\beta = 41.51$).[17] Based on electrostatic interactions, the carboxylate donor in the 7th coordinate site is expected to form a stronger bond to the highly charged Zr^{4+} ion than an aquo ligand. In an experimental situation, the chelate effect is also likely to increase the kinetic stability of the 7-coordinate complexes formed with heptadentate ligands compared with the $[ZrDFO(H_2O)]^+$ species.

Similar results were obtained with the three model complexes, Zr-**1**, Zr-**2**, and Zr-**3** where the new carboxylate donor

Table 1 Calculated reaction energetics for the formation of four different Zr^{4+} complexes with 7-coordinate geometry in the first coordination sphere of the metal cation

B3LYP/DGDZVP/PCM	Calculated reaction energetics for Zr-complex formation						
7-Coordinate complexes (model DFO)	$\Delta\varepsilon$ (SCF)/ kJ mol^{-1}	ΔZPE/ kJ mol^{-1}	ΔG/ kJ mol^{-1}	ΔH/ kJ mol^{-1}	ΔS/ J K^{-1} mol^{-1}	Calculated pseudo $\log\beta'$	Estimated $\log\beta$[17]
$[ZrDFO(H_2O)]^+$ (ref. 17)	−684.0	9.1	−730.0	−681.6	162.3	127.87	41.51
ZrDFO-succinate	−730.8	10.9	−774.9	−729.5	264.7	135.74	45.47
ZrDFO-Gly-Gly-Glu-C(O)Me (model Zr-**1**)	−758.9	10.4	−797.0	−756.2	264.6	139.61	47.42
ZrDFO-Gly-Glu-Gly-C(O)Me (model Zr-**2**)	−763.5	7.9	−810.5	−761.9	264.7	141.98	48.61
ZrDFO-Glu-Gly-Gly-C(O)Me (model Zr-**3**)	−749.5	8.0	−798.7	−746.8	264.7	139.90	47.57

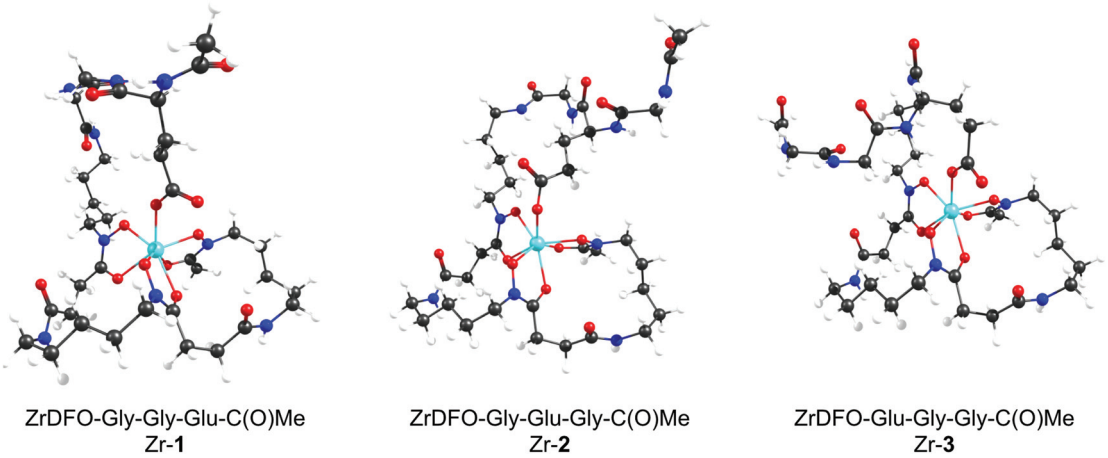

Fig. 2 Optimised structures of the three model Zr complexes.

atom stabilises the complex with respect to $[ZrDFO(H_2O)]^+$ by between −67.0 and −80.5 kJ mol^{-1}. In each case, the additional carboxylate donor ligand occupies the more stable pseudo-axial site. Complexation of Zr^{4+} ions by DFO-Gly-Gly-Glu-PEG_3-ArN_3 (**1**) and DFO-Glu-Gly-Gly-PEG_3-ArN_3 (**3**) gave equivalent estimated thermodynamic stability constants of 47.42 and 47.57, respectively. In contrast, DFO-Gly-Glu-Gly-PEG_3-ArN_3 (**2**) appears to form a slightly more stable complex ($\log\beta$ = 48.61) which is even higher than the predicted formation constants for some of the latest octadentate models.[17] From the optimised structure analysis (Fig. 2) it is evident that the extra carboxylate function is tightly bound to the Zr^{4+} cation which further explains the high values obtained for the calculated thermodynamic stability constants. We note that since the Zr^{4+} ion is very small, with an ionic radius of ~0.072 nm, it is not universally true that higher denticity (*e.g.* octadentate) ligands will form more stable complexes.[22] Rather, for these high denticity ligands where coordination number range from 6–8, the overall thermodynamic stability of the Zr^{4+} complex is the result of electrostatic attractions between the ligand and the metal ion, as well as electrostatic repulsions induced between the donor atoms of the ligand and steric strain induced in the complex when wrapping the ligand around the central metal ion. Solvation factors also play a role. The destabilising effect of steric strain can be observed when comparing the estimated formation constants of model complexes Zr-**1** and Zr-**3** *versus* the more stable model Zr-**2**. From these calculations, it appears that DFO-Gly-Glu-Gly-PEG_3-ArN_3 (**2**) is a potential candidate for the development of ^{89}Zr-radiolabelled mAbs.

^{89}Zr-Radiolabelling

Next, we explored the ^{89}Zr-radiolabelling of the 3 different DFO-based chelates (**1–3**) as well as a hexadentate control compound DFO–PEG_3–ArN_3 (compound **4**), the details of which were reported elsewhere.[25,33] Radiolabelling reactions to prepare [^{89}Zr]ZrDFO-PEG_3-complexes ([^{89}Zr]Zr-**1**, [^{89}Zr]Zr-**2**, [^{89}Zr]Zr-**3**, and [^{89}Zr]Zr-**4**$^+$) were accomplished by the addition of an aliquot of neutralised $[^{89}Zr][Zr(C_2O_4)_4]^{4-}$ stock solution (10 μL, ~5 MBq) to an aqueous solution of the corresponding DFO compound (**1–4**, 10 μL of a 3.32 mM stock [10% DMSO in H_2O]). The reactions were diluted to 50 μL by the addition of metal ion free (Chelex-treated) water and the pH was adjusted to 8.0–8.4 by adding aliquots of 0.1 M Na_2CO_3 (aq.). Reactions were stirred gently at room temperature for 5 minutes and ^{89}Zr-radiolabelling was characterised by using radioactivity measurements combined with both instant thin-layer chromatography (radio-iTLC) and high-performance liquid chromatography (radio-HPLC) methods (Fig. 3). Quantitative ^{89}Zr-radiolabelling yields were obtained in <5 min, and in all cases, the radiochemical purity (RCP) of the product was >95% (measured by integration of the decay-corrected HPLC chromatograms).

Stability studies *in vitro*

To gain further information about the effect of introducing a new coordinating carboxylate donor group at different positions on the stability of the radiocomplexes toward demetallation, we performed several challenge experiments. First, the stability of the radiometallated complexes towards decomplexation in human serum at 37 °C for 72 h was investigated. In addition, we performed classic ligand challenge experiments with excess EDTA (100 eq., pH7.4), and transmetallation challenge experiments using $FeCl_3$ (1 eq., pH7.4).[38] The complex stability was measured by radio-iTLC after incubating the solutions in PBS (pH7.4) for 72 h incubation. Experiments were performed in triplicate and a bar chart summarising the results is depicted in Fig. 4 (see also ESI Table S1†).

All radiocomplexes showed similar stability in the human serum challenge. [^{89}Zr]Zr-**1** was slightly less stable with respect to loss of the metal ion from the chelate but remained 91.4 ± 1.88% intact after 72 h. In comparison, [^{89}Zr]Zr-**2**, [^{89}Zr]Zr-**3**, and [^{89}Zr]Zr-**4**$^+$ were found to be 92.8 ± 1.66%, 93.7 ± 2.54% and 95.4 ± 1.34% intact, respectively. Interestingly, for the ligand challenge experiments [^{89}Zr]Zr-**1** suffered from highest degree of instability with 64.8 ± 15.4% transchelation to give

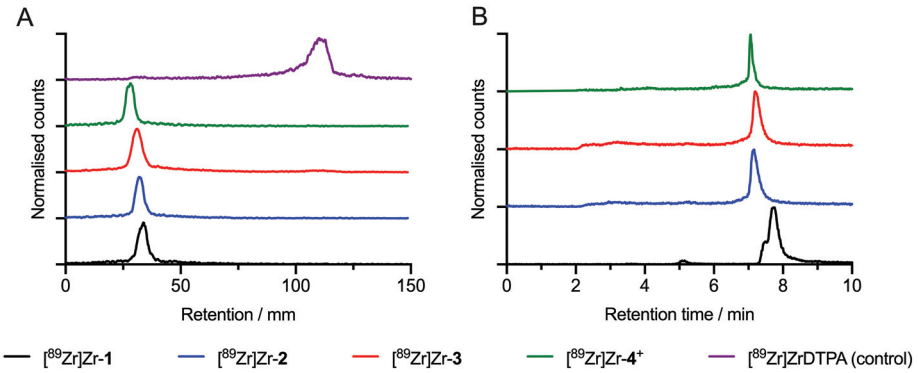

Fig. 3 Radioactive chromatography showing: (A) radio-iTLC chromatograms of [^{89}Zr]Zr-**1** (black trace), [^{89}Zr]Zr-**2** (blue trace), [^{89}Zr]Zr-**3** (red trace), and [^{89}Zr]Zr-**4**$^{+}$ (green trace). The elution profile of [^{89}Zr][Zr(DTPA)]$^{-}$ (purple trace) is shown as a control. (B) Radio-HPLC chromatograms of [^{89}Zr]Zr-**1** to [^{89}Zr]Zr-**4**$^{+}$ (black to green traces).

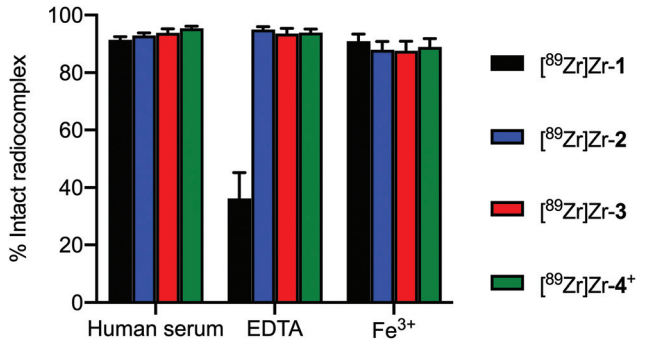

Fig. 4 Bar chart showing the stability of the ^{89}Zr-radiolabelled complexes (formed from chelates **1–4**) under different challene conditions. The plot shows the percentage of the intact radiocomplex (n = 3) measured by radio-iTLC.

the [^{89}Zr][Zr(EDTA)]$^{-}$ after 72 h. The three other complexes were equivalently stable with only an ~7% loss of ^{89}Zr-activity after 72 h incubation. Finally, all the radiocomplexes possess similar stability with respect to transmetallation with Fe^{3+} ions. In each case, after 72 h incubation with 1 equivalent of Fe^{3+} ions, only a minor fraction of ~13% of the $^{89}Zr^{4+}$ ion was released. One point to note is that the measured stability of the ZrDFO complex (and indeed other Zr-complexes that feature hydroxamate donors) is highly dependent on the pH of the test samples.[39] Hydroxamate groups have pKa values around 6–9, whereas most carboxylic acids have pKa values in the range 3.5–4.5.[40,41] Hence, if the pH of the ligand challenge experiment is not tightly controlled, a slight decrease below *ca.* pH7 will lead to transchelation in the presence of excess EDTA (or DTPA). In our hands, and in contrast to some recent reports,[42,43] the hexadentate ZrDFO complex is stable at pH7.4 in PBS. These experiments indicate that Zr-complexes formed with the new heptadentate chelates **1–3** show similar kinetic stability toward metal ion release, transchelation or transmetallation to that of a classic ZrDFO-species (here represented by Zr-**4**$^{+}$).

One-pot photoradiolabelling of MetMAb™

Based on the stability studies and the high calculated thermodynamic formation constant of the Zr-complex formed with DFO-Gly-Glu-Gly-PEG$_3$-ArN$_3$ (**2**), we decided to perfom the light-induced ^{89}Zr-radiolabelling reaction using MetMAb™ (a fully formulated clinical grade solution containing the one-armed monoclonal antibody onartuzumab; Scheme 2).[32] Initially, we evaluated the complexation of [^{89}Zr][Zr(C$_2$O$_4$)$_4$]$^{4-}$ with compound **2** by using radio-iTLC (radio-iTLC, Fig. 5A, orange trace). As shown above, a radiochemical conversion (RCC) >99% to give [^{89}Zr]Zr-**2** was obtained in <5 min at room temperature and at pH 8.0–8.4. Then, an aliquot of MetMAb™ (21.2 nmol of onartuzumab protein, MW 99.16 kDa, and containing all formulation components in their native concentrations: 10 nmol L^{-1} histidine succinate, 106 nmol L^{-1} trehalose dihydrate, 0.02% polysorbate 20, pH 5.7) was added. The initial chelate-to-protein ratio was fixed at ~1.05 : 1.0 and the reaction pH was checked (8.0–8.4) before adjusting the final volume to 150 μL by using metal ion free water. The reactions were gently stirred and irradiated at 395 nm at room temperature for 15 min. No change in the temperature of the reaction mixture was observed during the irradiation. Aliquots of the crude reaction mixture were kept for analysis and fractions were purified manually on a size-exclusion chromatography (SEC) gel filtration (PD-10) column. Crude and purified samples were analysed by radio-iTLC (Fig. 5A), analytical PD-10-SEC (Fig. 5B), and automated SEC-HPLC coupled to a gel filtration column (Fig. 5C). In the analysis of the crude and purified samples of [^{89}Zr]Zr-**2**-onartuzumab, radio-iTLC confirmed that the ^{89}Zr activity did not dissociate from the metal binding chelate, as shown by retention of activity at the baseline (R_f = 0.0, Fig. 6A black and blue traces). In this set of experiments, the purification of [^{89}Zr]Zr-**2**-onartuzumab lacked optimal separation when using manual PD-10 columns (Fig. 5C, green trace) and gave a RCP of 61%. Therefore, crude samples of [^{89}Zr]Zr-**2**-onartuzumab were purified by using spin-filtration (Amicon spin filters equipped with permeable membranes with a molecular weight cutoff of 100 kDa) to

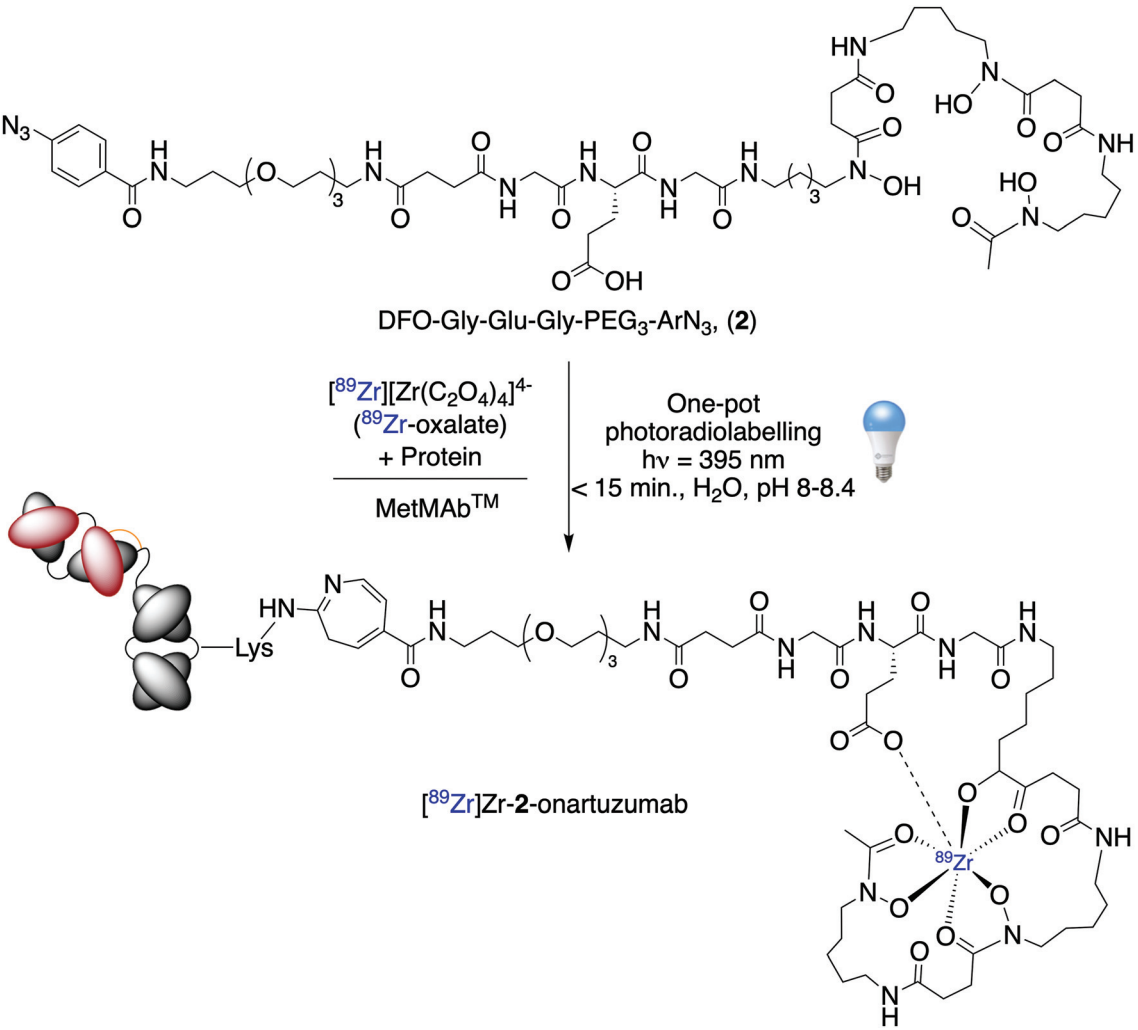

Scheme 2 One-pot, light-induced protein conjugation and ^{89}Zr-radiolabelling of fully formulated onartuzumab (MetMAb™) by using photochemical activation of DFO-Gly-Glu-Gly-PEG$_3$-ArN$_3$ (**2**).

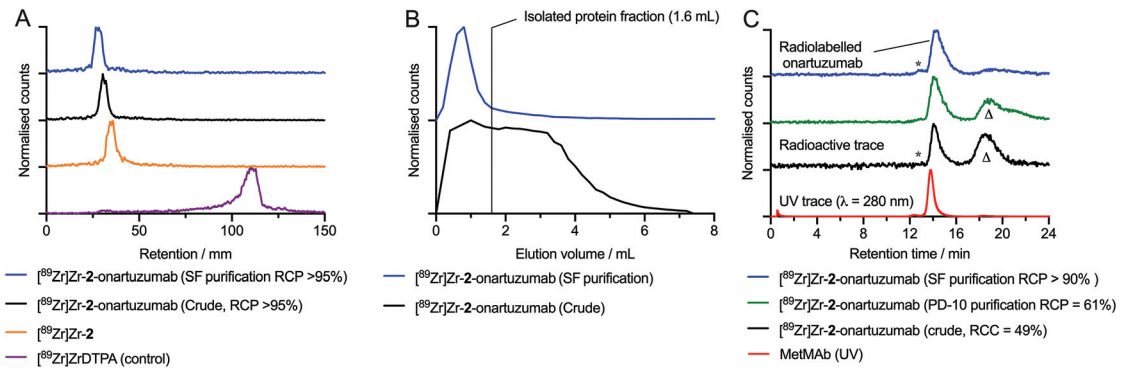

Fig. 5 Radioactive chromatography data showing: (A) radio-iTLC chromatograms of [^{89}Zr]Zr-**2** (organe trace), the crude (black trace) and purified (blue trace) samples of the protein labelled [^{89}Zr]Zr-**2**-onartuzumab, and the control [^{89}Zr][Zr(DTPA)]$^{-}$ (purple trace). (B) Analytical SEC (PD-10) elution profiles showing the crude (black trace) and purified (blue trace) samples of [^{89}Zr]Zr-**2**-onartuzumab. (C) Radioactive and electronic absorption HPLC chromatograms acquired by using automated SEC gel-filtration showing analysis of the crude (black trace) and purified (green and blue radiotraces) samples of [^{89}Zr]Zr-**2**-onartuzumab. As a reference, the chromatogram of the stock solution of MetMAb is also presented (red trace). Note (*) corresponds to a protein aggregate fraction; (Δ) corresponds to the small-molecule byproducts obtained after photolysis of [^{89}Zr]Zr-**2** (mainly assigned to the hydrolysis product [^{89}Zr]Zr-**2**-azepin-2-ol).[44]

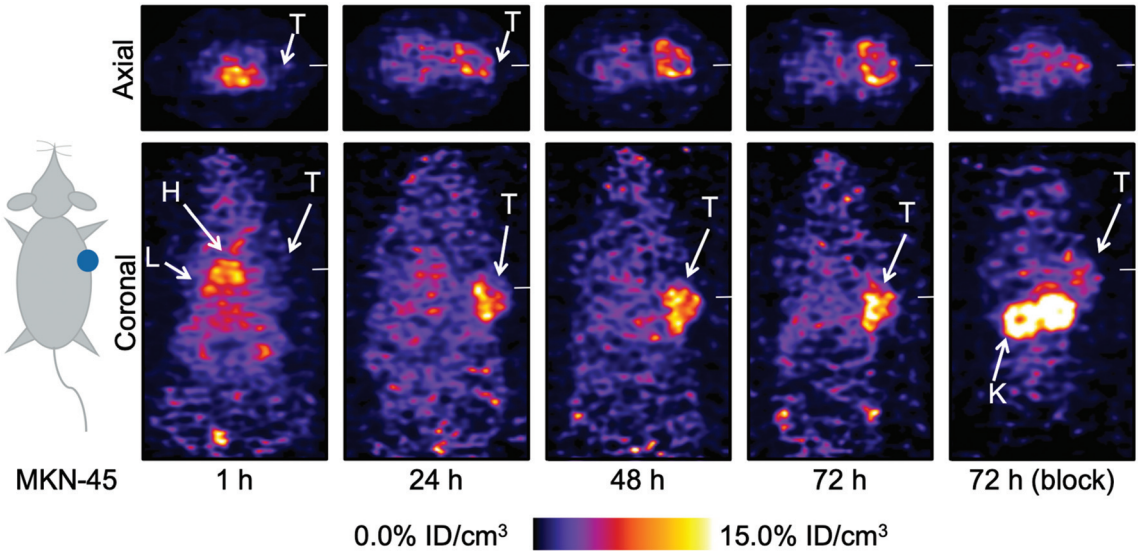

Fig. 6 Coronal and axial PET images taken through the centre of the tumours showing the spatial distribution of [^{89}Zr]Zr-**2**-onartuzumab over time after intravenous administration in mice bearing subcutaneous MKN-45 tumours on the right flank. T = Tumour, H = Heart, L = Liver, K = Kidneys.

remove the radiolabelled small-molecule components (labelled as Δ, and mainly assigned to the hydrolysed by-products produced after photolysis of the ArN_3 group[44]). After spin-filtration, [^{89}Zr]Zr-**2**-onartuzumab was obtained with a decay-corrected (d.c.) radiochemical yield of 36.4 ± 2.4% (n = 2 independent measurements) and a RCP >90%, which was sufficient to allow further evaluation *in vivo*.

Small-animal PET imaging. Small-animal PET imaging studies were performed in female athymic nude mice bearing subcutaneous MKN-45 human xenografts on the right shoulder (Fig. 6). Maximum intensity projection images are shown in ESI Fig. S28.† Two groups of animals corresponding to a normal (n = 3 mice) and a competitive inhibition or blocking experiment (n = 3) received between 0.18 and 0.22 MBq of [^{89}Zr]Zr-**2**-onartuzumab *via* intravenous tail-vein injection. The normal group received between 59–72 μg of onartuzumab per animal while the blocking group received the same activity dose but a ~15 fold higher protein dose to modulate the tumour uptake by saturating the available c-Met receptors in the xenograft. PET images were recorded at multiple time points between 0–72 h post-radiotracer administration. Quantitative volume-of-interest (VOI) analysis from the PET

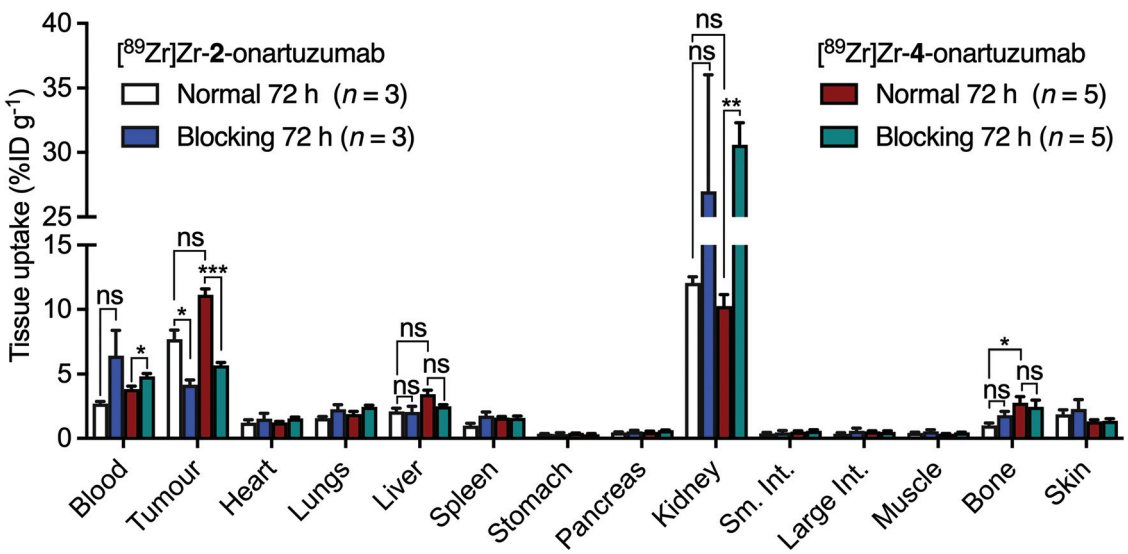

Fig. 7 Bar chart showing *ex vivo* biodistribution data (%ID g^{-1}) for the uptake of [^{89}Zr]Zr-**2**-onartuzumab (normal group, white; blocking group, blue) and the control compound [^{89}Zr]Zr-**4**-onartuzumab (normal group, red; blocking group, green) in mice bearing MKN-45 tumours. Note: Data obtained for [^{89}Zr]Zr-**4**-onartuzumab were originally reported in ref. 33.

images (Fig. S29†) revealed accumulation of the radiotracer in the tumours of the normal group which reached 9.02 ± 0.31% ID cm^{-3} by 72 h post-injection. The tumour uptake in the blocking group decreased by ~44% to 3.96 ± 0.89%ID cm^{-3} (*P*-value <0.001). The blocking effect was clearly visualised in the tomographic and maximum intensity PET images (Fig. 6 and Fig. S28†) which provided confirmation that [^{89}Zr]Zr-**2**-onartuzumab remained biologically active *in vivo* and specific toward the c-Met biomarker. The results obtained here are similar to the *in vivo* behaviour of the hexadentate [^{89}Zr]ZrDFO-PEG_3-azepin-onartuzumab (corresponding to the [^{89}Zr]Zr-**4**-onartuzumab control compound) reported previously.[33]

Biodistribution studies *ex vivo*. After the final imaging time point, animals were euthanised and biodistribution studies were performed at 72 h post-injection (Fig. 7, ESI Table S2 and Fig. S30, 31†). *Ex vivo* analysis demonstrated accumulation of the tracer in the tumours of the normal group reaching 7.69 ± 1.23%ID g^{-1} compared with 4.18 ± 0.64%ID g^{-1} for the blocking group (~45% decrease; *P*-value <0.05). Biodistribution data were consistent with the quantitative VOI analysis from the PET images. Bone uptake remained extremely low in both groups, with only 1.01 ± 0.34%ID g^{-1} and 1.80 ± 0.53%ID g^{-1} for the normal and blocking group, respectively. As a comparison, the bone uptake of the control compound [^{89}Zr]Zr-**4**-onartuzumab was ~2.5 times higher (normal group: 2.77 ± 1.07%ID g^{-1} [*P*-value <0.05], and blocking group: 2.46 ± 1.07%ID g^{-1}), which highlights the improved stability of [^{89}Zr]Zr-**2**-onartuzumab *in vivo*.[33] With the exception of radioactivity accumulation in the kidneys, which showed uptake that is dependent on the adminsitered protein mass, accumulation in other background organs was relatively low (<2%ID g^{-1}) for both tracers. Overall, [^{89}Zr]Zr-**2**-onartuzumab provides specific tumour targeting and high tumour-to-organ contrast on the PET pictures and from the biodisitrbution analysis. The results confirm that heptadentate complexes of ^{89}Zr display improved stability *in vivo* and are promising candidates for future ^{89}Zr-radiotracer design.

Conclusion

In this study, we developed a versatile tripeptide (Gly-Gly-Glu) scaffold using solid-phase peptide synthesis for synthesising bifunctional DFO conjugates with the possibility to expand the donor atom set to 7. We used DFT calculations to predict the thermodynamic stability constants of the Zr-complexes with the new heptadentate chelates. These calculations highlighted that introducing a carboxylate group as a 7th donor atom in a pseudo-axial coordination site resulted in higher thermodynamic stability constants than for the hexadentate [ZrDFO(H_2O)]$^+$ species. Experiments *in vitro* revealed that the introduction of a 7th-coordinating group does not significantly impact the stability of the radiocomplexes. However, we demonstrated that the stability of [^{89}Zr]Zr-**2**-onartuzumab was superior to the control compound bearing the hexadentate DFO chelate, giving reduced bone uptake *in vivo.* Based on these data, we propose that new Zr–chelate design should not be restricted to octadentate systems but that scientists should also consider exploring the potential of heptadentate ligands.

Materials and methods

Full details on the materials and methods used, as well as characterisation data are provided in the electronic ESI.†

Author contributions

A.G. and J.P.H. designed the project. A.G. performed all the experiments. J.P.H. performed the DFT calculations. A.G., A.O. and J.P.H. analysed the data. J.P.H. supervised the project. A.G. and J.P.H. prepared the manuscript which was reviewed by all the authors. All authors have read and approved the final version of this work.

Conflicts of interest

There are no conflicts to declare.

Acknowledgements

J. P. H. thanks the Swiss National Foundation (SNSF Professorship PP00P2_163683 and PP00P2_190093) and the European Union's Horizon 2020 Research and Innovation Programme (ERC-StG-2015, 676904, NanoSCAN; ERC-CoG-2020, 101001734, PhotoPHARMA) for financial support. The work has been supported in part by a grant from the French National Agency for research called "Investissements d'Avenir" Labex IRON n°ANR-11-LABX-0018-01. We thank Dr Florian Moulin for help in the synthesis.

References

1 J. R. Dilworth and S. I. Pascu, The Chemistry of PET Imaging with Zirconium-89, *Chem. Soc. Rev.*, 2018, **47**(8), 2554–2571, DOI: **10.1039/C7CS00014F**.
2 J. P. Holland, M. J. Williamson and J. S. Lewis, Unconventional Nuclides for Radiopharmaceuticals, *Mol. Imaging*, 2010, **9**(1), 1–20.
3 R. G. Pearson, Hard and Soft Acids and Bases, *J. Am. Chem. Soc.*, 1963, **85**(22), 3533–3539, DOI: **10.1021/ja00905a001**.
4 B. N. McKnight and N. T. Viola-Villegas, ^{89}Zr-ImmunoPET Companion Diagnostics and Their Impact in Clinical Drug Development, *J. Labelled Compd. Radiopharm.*, 2018, **61**(9), 727–738, DOI: **10.1002/jlcr.3605**.
5 A.-L. N. Niemeijer, D. E. Oprea-Lager, M. C. Huisman, O. S. Hoekstra, R. Boellaard, B. J. de W. der Veen, I. Bahce, D. J. Vugts, G. A. M. S. van Dongen, E. Thunnissen, E. F. Smit and A. J. de Langen, Study of ^{89}Zr-Pembrolizumab

PET/CT in Patients With Advanced-Stage Non–Small Cell Lung Cancer, *J. Nucl. Med.*, 2022, **63**, 362–367, DOI: **10.2967/jnumed.121.261926**.

6 V. Liapis, W. Tieu, S. E. Rudd, P. S. Donnelly, N. L. Wittwer, M. P. Brown and A. H. Staudacher, Improved Non-Invasive Positron Emission Tomographic Imaging of Chemotherapy-Induced Tumor Cell Death Using Zirconium-89-Labeled APOMAB®, *EJNMMI Radiopharm. Chem.*, 2020, **5**, 27, DOI: **10.1186/s41181-020-00109-6**.

7 I. Verel, G. W. M. Visser, R. Boellaard, M. Stigter-van Walsum, G. B. Snow and G. A. van Dongen, ^{89}Zr Immuno-PET: Comprehensive Procedures for the Production of ^{89}Zr-Labeled Monoclonal Antibodies, *J. Nucl. Med.*, 2003, **44**(8), 1271–1281.

8 J. P. Holland, G. Normand, A. Ruggiero, J. S. Lewis and J. Grimm, Intraoperative Imaging of Positron Emission Tomographic Radiotracers Using Cerenkov Luminescence Emissions, *Mol. Imaging*, 2011, **10**(3), 177–186.

9 J. P. Holland, V. Divilov, N. H. Bander, P. M. Smith-Jones, S. M. Larson and J. S. Lewis, ^{89}Zr-DFO-J591 for ImmunoPET of Prostate-Specific Membrane Antigen Expression in Vivo, *J. Nucl. Med.*, 2010, **51**(8), 1293–1300, DOI: **10.2967/jnumed.110.076174**.

10 F. Guérard, Y.-S. Lee, R. Tripier, L. P. Szajek, J. R. Deschamps and M. W. Brechbiel, Investigation of Zr(IV) and ^{89}Zr(IV) Complexation with Hydroxamates: Progress towards Designing a Better Chelator than Desferrioxamine B for Immuno-PET Imaging, *Chem. Commun.*, 2013, **49**(10), 1002–1004, DOI: **10.1039/C2CC37549D**.

11 A. Bianchi and M. Savastano, Comment on "Investigation of Zr(IV) and ^{89}Zr(IV) Complexation with Hydroxamates: Progress towards Designing a Better Chelator than Desferrioxamine B for Immuno-PET Imaging" by F. Guérard, Y.-S. Lee, R. Tripier, L. P. Szajek, J. R. Deschamps and M. W. Brechbiel, *Chem. Commun.*, 2013, **49**, 1002, *Chem. Commun.*, 2020, **56**(83), 12664–12666, DOI: **10.1039/D0CC01189D**.

12 F. Guérard, Y.-S. Lee, R. Tripier, L. P. Szajek, J. R. Deschamps and M. W. Brechbiel, Reply to the 'Comment on "Investigation of Zr(IV) and ^{89}Zr(IV) Complexation with Hydroxamates: Progress towards Designing a Better Chelator than Desferrioxamine B for Immuno-PET Imaging"' by A. Bianchi and M. Savastano, *Chem. Commun.*, 2020, **56**, D0CC01189D, *Chem. Commun.*, 2020, **56**(83), 12667–12668, DOI: **10.1039/D0CC03594G**.

13 M. Savastano, C. Bazzicalupi, G. Ferraro, E. Fratini, P. Gratteri and A. Bianchi, Tales of the Unexpected: The Case of Zirconium(IV) Complexes with Desferrioxamine, *Molecules*, 2019, **24**(11), 2098, DOI: **10.3390/molecules24112098**.

14 M. Savastano, F. Boscaro and A. Bianchi, Metal Coordination Properties of a Chromophoric Desferrioxamine (DFO) Derivative: Insight on the Coordination Stoichiometry and Thermodynamic Stability of Zr^{4+} Complexes, *Molecules*, 2022, **27**(1), 184, DOI: **10.3390/molecules27010184**.

15 Y. Toporivska and E. Gumienna-Kontecka, The Solution Thermodynamic Stability of Desferrioxamine B (DFO) with Zr(IV), *J. Inorg. Biochem.*, 2019, **198**, 110753, DOI: **10.1016/j.jinorgbio.2019.110753**.

16 E. E. Racow, J. J. Kreinbihl, A. G. Cosby, Y. Yang, A. Pandey, E. Boros and C. J. Johnson, General Approach to Direct Measurement of the Hydration State of Coordination Complexes in the Gas Phase: Variable Temperature Mass Spectrometry, *J. Am. Chem. Soc.*, 2019, **141**(37), 14650–14660, DOI: **10.1021/jacs.9b05874**.

17 J. P. Holland, Predicting the Thermodynamic Stability of Zirconium Radiotracers, *Inorg. Chem.*, 2020, **59**(3), 2070–2082, DOI: **10.1021/acs.inorgchem.9b03515**.

18 K. L. Summers, E. K. Sarbisheh, A. Zimmerling, J. J. H. Cotelesage, I. J. Pickering, G. N. George and E. W. Price, Structural Characterization of the Solution Chemistry of Zirconium(IV) Desferrioxamine: A Coordination Sphere Completed by Hydroxides, *Inorg. Chem.*, 2020, **59**(23), 17443–17452, DOI: **10.1021/acs.inorgchem.0c02725**.

19 N. B. Bhatt, D. N. Pandya and T. J. Wadas, Recent Advances in Zirconium-89 Chelator Development, *Molecules*, 2018, **23**(3), 638, DOI: **10.3390/molecules23030638**.

20 J. R. Dilworth and S. I. Pascu, The Chemistry of PET Imaging with Zirconium-89, *Chem. Soc. Rev.*, 2018, **47**(8), 2554–2571, DOI: **10.1039/C7CS00014F**.

21 I. V. J. Feiner, M. Brandt, J. Cowell, T. Demuth, D. Vugts, G. Gasser and T. L. Mindt, The Race for Hydroxamate-Based Zirconium-89 Chelators, *Cancers*, 2021, **13**(17), 4466, DOI: **10.3390/cancers13174466**.

22 J. P. Holland, *The Radiochemistry of Zirconium, in Handbook of Radiopharmaceuticals*, John Wiley & Sons, Ltd, 2020, pp, 343–374. DOI: **10.1002/9781119500575.ch11**.

23 P. Dennler, E. Fischer and R. Schibli, Antibody Conjugates: From Heterogeneous Populations to Defined Reagents, *Antibodies*, 2015, **4**(3), 197–224, DOI: **10.3390/antib4030197**.

24 J. P. Holland, M. Gut, S. Klingler, R. Fay and A. Guillou, Photochemical Reactions in the Synthesis of Protein–Drug Conjugates, *Chem. – Eur. J.*, 2020, **26**(1), 33–48, DOI: **10.1002/chem.201904059**.

25 A. Guillou, D. F. Earley, M. Patra and J. P. Holland, Light-Induced Synthesis of Protein Conjugates and Its Application in Photoradiosynthesis of ^{89}Zr-Radiolabeled Monoclonal Antibodies, *Nat. Protoc.*, 2020, **15**(11), 3579–3594, DOI: **10.1038/s41596-020-0386-5**.

26 M. Patra, S. Klingler, L. S. Eichenberger and J. P. Holland, Simultaneous Photoradiochemical Labeling of Antibodies for Immuno-Positron Emission Tomography, *iScience*, 2019, **13**, 416–431, DOI: **10.1016/j.isci.2019.03.004**.

27 R. Fay, M. Gut and J. P. Holland, Photoradiosynthesis of ^{68}Ga-Labeled HBED-CC-Azepin-MetMAb for Immuno-PET of c-MET Receptors, *Bioconjugate Chem.*, 2019, **30**(6), 1814–1820, DOI: **10.1021/acs.bioconjchem.9b00342**.

28 R. Fay, A. Linden and J. P. Holland, PhotoTag: Photoactivatable Fluorophores for Protein Labeling, *Org.*

Lett., 2020, **22**(9), 3499–3503, DOI: **10.1021/acs.orglett.0c00957**.

29 A. Guillou, E. Nisli, S. Klingler, A. Linden and J. P. Holland, Photoactivatable Fluorescent Tags for Dual-Modality Positron Emission Tomography Optical Imaging, *J. Med. Chem.*, 2022, **65**(1), 811–823, DOI: **10.1021/acs.jmedchem.1c01899**.

30 W. T. Borden, N. P. Gritsan, C. M. Hadad, W. L. Karney, C. R. Kemnitz and M. S. Platz, The Interplay of Theory and Experiment in the Study of Phenylnitrene, *Acc. Chem. Res.*, 2000, **33**(11), 765–771, DOI: **10.1021/ar990030a**.

31 S. Klingler and J. P. Holland, Automated Light-Induced Synthesis of ^{89}Zr-Radiolabeled Antibodies for Immuno-Positron Emission Tomography, *Sci. Rep.*, 2022, **12**(1), 668, DOI: **10.1038/s41598-021-04626-5**.

32 M. Merchant, X. Ma, H. R. Maun, Z. Zheng, J. Peng, M. Romero, A. Huang, N. Yang, M. Nishimura, J. Greve, L. Santell, Y.-W. Zhang, Y. Su, D. W. Kaufman, K. L. Billeci, E. Mai, B. Moffat, A. Lim, E. T. Duenas, H. S. Phillips, H. Xiang, J. C. Young, G. F. Vande Woude, M. S. Dennis, D. E. Reilly, R. H. Schwall, M. A. Starovasnik, R. A. Lazarus and D. G. Yansura, Monovalent Antibody Design and Mechanism of Action of Onartuzumab, a MET Antagonist with Anti-Tumor Activity as a Therapeutic Agent, *Proc. Natl. Acad. Sci. U. S. A.*, 2013, **110**(32), E2987–E2996, DOI: **10.1073/pnas.1302725110**.

33 A. Guillou, D. F. Earley and J. P. Holland, Light-Activated Protein Conjugation and ^{89}Zr-Radiolabelling with Water-Soluble Desferrioxamine Derivatives, *Chem. – Eur. J.*, 2020, **26**(32), 7185–7189, DOI: **10.1002/chem.202001755**.

34 B. J. Intorre and A. E. Martell, Aqueous Zirconium Complexes. II. Mixed Chelates1, *J. Am. Chem. Soc.*, 1961, **83**(17), 3618–3623, DOI: **10.1021/ja01478a018**.

35 B. J. Intorre and A. E. Martell, Zirconium Complexes in Aqueous Solution. III. Estimation of Formation Constants, *Inorg. Chem.*, 1964, **3**(1), 81–87, DOI: **10.1021/ic50011a017**.

36 M. Sturzbecher-Hoehne, T. A. Choi and R. J. Abergel, Hydroxypyridinonate Complex Stability of Group (IV) Metals and Tetravalent f-Block Elements: The Key to the Next Generation of Chelating Agents for Radiopharmaceuticals, *Inorg. Chem.*, 2015, **54**(7), 3462–3468, DOI: **10.1021/acs.inorgchem.5b00033**.

37 Y. Toporivska, A. Mular, K. Piasta, M. Ostrowska, D. Illuminati, A. Baldi, V. Albanese, S. Pacifico, I. O. Fritsky, M. Remelli, R. Guerrini and E. Gumienna-Kontecka, Thermodynamic Stability and Speciation of Ga(III) and Zr(IV) Complexes with High-Denticity Hydroxamate Chelators, *Inorg. Chem.*, 2021, **60**(17), 13332–13347, DOI: **10.1021/acs.inorgchem.1c01622**.

38 C. J. M. Brown, M. P. Gotsbacher, R. Codd, C. J. M. Brown, M. P. Gotsbacher and R. Codd, Improved Access to Linear Tetrameric Hydroxamic Acids with Potential as Radiochemical Ligands for Zirconium(IV)-89 PET Imaging, *Aust. J. Chem.*, 2020, **73**(10), 969–978, DOI: **10.1071/CH19518**.

39 J. P. Holland and J. S. Lewis, Zirconium-89 chemistry in the design of novel radiotracers for immuno-PET, in *Technetium and Other Radiometals in Chemistry and Medicine*, ed. U. Mazzi, W. C. Eckelman and W. A. Volkert, Padova, Italy, 2010, pp. 187–192.

40 Y. K. Agrawal, Hydroxamic Acids and Their Metal Complexes, *Russ. Chem. Rev.*, 1979, **48**(10), 948, DOI: **10.1070/RC1979v048n10ABEH002422**.

41 L. A. Green, L. G. Sainsbury, B. Saville and M. Stansfield, 316. The Reactivity of Some Active Nucleophilic Reagents with Organophosphorus Anticholinesterases, *J. Chem. Soc. (Resumed)*, 1958, 1583–1587, DOI: **10.1039/JR9580001583**.

42 M. Brandt, J. Cowell, M. L. Aulsebrook, G. Gasser and T. L. Mindt, Radiolabelling of the Octadentate Chelators DFO* and OxoDFO* with Zirconium-89 and Gallium-68, *JBIC, J. Biol. Inorg. Chem.*, 2020, **25**(5), 789–796, DOI: **10.1007/s00775-020-01800-4**.

43 L. Southcott, L. Li, B. O. Patrick, H. Stephan, M. G. de Jaraquemada-Peláez and C. Orvig, [$^{Nat/89}$Zr][Zr(Pypa)]: Thermodynamically Stable and Kinetically Inert Binary Nonadentate Complex for Radiopharmaceutical Applications, *Inorg. Chem.*, 2021, **60**(23), 18082–18093, DOI: **10.1021/acs.inorgchem.1c02709**.

44 A. Guillou, D. F. Earley, S. Klingler, E. Nisli, L. J. Nüesch, R. Fay and J. P. Holland, The Influence of a Polyethylene Glycol Linker on the Metabolism and Pharmacokinetics of a ^{89}Zr-Radiolabeled Antibody, *Bioconjugate Chem.*, 2021, **32**(7), 1263–1275, DOI: **10.1021/acs.bioconjchem.1c00172**.